The American Association of Petroleum Geologists Bulletin
V. 69, No. 5 (May 1985), P. 699-709, 18 Figs., 3 Tables

Hydrothermics in the Wyoming Overthrust Belt[1]

GARY W. ZIELINSKI,[2,3] JAMES A. DRAHOVZAL,[2,4]
GAIL MORITZ DECOURSEY,[2,5] and JOSEPH M. RUPERTO[2,6]

ABSTRACT

A thermal study was made across a 25 km (15.5 mi) traverse of the Overthrust belt in southwestern Wyoming. Estimates of relative heat flow from temperature measurements made in shallow (< 30 m or 98 ft) boreholes reveal a systematic variation of at least 400 mW/m^2 (10 μcal/cm^2 sec) magnitude across the study area. The cause of this variation is believed to be forced convection of heat by moving ground water. Two relative heat-flow highs coincide with zones where structurally related faults, possibly providing avenues for vertical water flow, project to the surface. Between those two zones in a topographically elevated area, low and predominately negative temperature gradients were observed in opposite seasons. These shallow negative gradients are believed to exist seasonally in quasisteady state and could be indicative of a broad zone of ground-water recharge. The association of two relative heat-flow highs with the two major deep geologic structures implies either a direct vertical communication of deep and shallow ground water or a coupling of deeper and shallower ground-water systems. The two structures studied are hydrocarbon bearing and associated with Whitney Canyon and Ryckman Creek fields. The thermal measurements support the possibility that ascending waters have influenced the hydrocarbon migration and accumulation in these structures. Such measurements may be useful in delineating and understanding similar features in other areas.

INTRODUCTION

Theories on the hydrodynamic influence on oil and gas migration (Roberts, 1979; Toth, 1980) and the sensitivity of the earth's temperature field to ground-water movement (Bredehoeft and Papadopulos, 1965) have led to the use of shallow thermal measurements specifically to test these theories (Zielinski and Bruchhausen, 1983). The techniques employed were similar to those first applied by Lee (1977) and Lee and Cohen (1979) to delineate the Salton Sea geothermal area. To optimize their chances of success, Zielinski and Bruchhausen (1983) chose their study area, Tierra del Fuego, South America, partly on the basis of optimum environmental conditions. Consequently, several extremely shallow (2 m or 6.6 ft) relative heat-flow measurements could be explained by the occurrence of deep-water discharge coincident with individual hydrocarbon-associated basement structures. This conclusion, which was consistent with suggested hydrothermics and hydrocarbon generation and migration in the Magellan basin, was based, however, on a limited number of measurements.

In the autumn of 1980 the opportunity arose to attempt 25 new relative heat-flow measurements in the western Overthrust belt in boreholes ranging in depth to nearly 30 m (98 ft). This represents a significant increase in the data base from that of Zielinski and Bruchhausen (1983), and the increased depth of measurement might be expected to produce more reliable determinations. It was also desirable because topographic relief and lateral changes in vegetation and lithology are considerably greater (and more likely to create temperature noise) in the present study area than in Tierra del Fuego.

The area under investigation is located in the southwest corner of Wyoming near the Utah state line and within the western Overthrust belt (Figure 1). Thermal measurements were made in boreholes located at various positions along line AA′ (Figure 1), which traverses the area's predominately north-south structural trend. A structure profile based on seismic and well data is given in Figure 2 for the segment of line AA′ that crosses fold structure associated with the Whitney Canyon and Ryckman Creek fields. Both structures occur within the Absaroka thrust sheet. The Whitney Canyon (left in Figure 2) structure is an asymmetric faulted anticline with predominately gas production from lower Mesozoic and Paleozoic strata. In contrast, the Ryckman Creek structure is overturned with its fold axis dipping to the west. Associated hydrocarbon production is predominately oil and condensate from the Jurassic Nugget Formation.

THERMAL MEASUREMENTS

Site preparation for the measurements was identical to that suggested by Lee (1977) and Lee and Cohen (1979) for their onshore stations. PVC tubing of 1/2-in. diameter was inserted into each borehole, and the annulus backfilled. Allowing for sufficient time to elapse after drilling, measurements were obtained by lowering a thermistor probe into the casing and recording at discrete depths. Many of

[1]Manuscript received, February 22, 1984; accepted, November 12, 1984.

[2]Gulf Research and Development Co., P.O. Box 37048, Houston, Texas 77236.
[3]Now at Department of Applied Science, Brookhaven National Laboratory, Upton, New York 11973.
[4]Now at ARCO Oil and Gas Co., P.O. Box 2819, Dallas, Texas 75221.
[5]Now at Marathon Oil Co., P.O. Box 3128, Houston, Texas 77001.
[6]Now at Maryland Bureau of Mines, 69 Hill Street, Frostburg, Maryland 21532.

We gratefully acknowledge careful reviews by B. Hitchon, H. Meyer, I. Lerche, C. Kendall, and W. Roberts, III. Gulf's participation in this experiment can be partly attributed to concepts expounded by Bill Roberts over at least the past 25 years. The writers dedicate this paper to Bill. We thank Gulf Research and Development Company for granting permission to publish. Support for completion of this work was given by Department of Energy Contract DE-AC02-76CH00016.

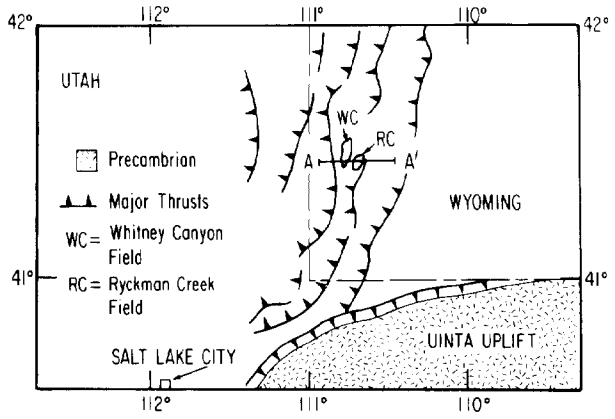

Figure 1—Generalized geology and location map for Whitney Canyon–Ryckman Creek study area. Thermal measurements were made along line AA′.

the holes were partially filled with water. In water, equilibration occurred usually within 5 min; for measurements in dry air, equilibration took on the order of 30 min in most cases. Details of the instrumentation and procedure are described by Zielinski and Bruchhausen (1983). The observed temperature profiles for all measured stations are shown in Figure 3. For a variety of reasons, the range in depth over which the measurements were made at each station varied so that relative heat-flow estimates were not possible for all stations. As an aid in obtaining a data reduction for the maximum number of sites, an additional constraint on the data was afforded by analysis of daily observations of surface air temperatures for 1 year prior to field measurements (Figure 4). The temperature data were obtained at the U.S. Weather Service station located in Evanston, Wyoming, less than 50 km (31 mi) south of the study area.

The temperature values shown in Figure 3 were obtained in a depth interval where it is likely that the dominant transient component of the temperature field is due to the seasonal fluctuation of surface temperature. The indirect method of Lee (1977) was used to remove this transient component from the temperature profiles and to obtain an estimate of the mean equilibrium geothermal gradient and a value of the average thermal diffusivity over the depth interval for each station. The data reduction scheme (described in more detail by Lee, 1977; Lee and Cohen, 1979; Zielinski and Bruchhausen, 1983) makes use of a linearized form of the solution for heat conduction in a homogeneous half-space with sinusoidally varying surface temperature (period = 1 year),

$$T_{ji} = T_s + gz_i + \delta_j x_i + \epsilon_j y_i \qquad (1)$$

where

$$\delta_j = A \sin \omega(t_j - t_o),$$
$$\epsilon_j = -A \cos \omega(t_j - t_o),$$

and

$$x_i = \exp(-z_i[\omega/2\mu]^{1/2}) \cos(z_i[\omega/2\mu]^{1/2}),$$
$$y_i = \exp(-z_i[\omega/2\mu]^{1/2}) \sin(z_i[\omega/2\mu]^{1/2}),$$

and T_{ji} are the temperatures measured at depths z_i. T_s is the mean surface temperature, A is the amplitude of the annual surface-temperature variation, g is the geothermal gradient, ω is the angular velocity of the annual temperature variation (2×10^{-7} sec^{-1}), t_o is the time when $T(z = 0) = T_s$, t_j is time of measurement, and μ is thermal diffusivity. A minimum root-mean-square (RMS) error solution to equation 1 is sought after assigning discrete values of μ ranging from 0.001 to 0.020 cm^2 sec^{-1} in increments of 10^{-4} cm^2 sec^{-1}, which covers the range of values normally observed for soils and rock (e.g., Kappelmeyer and Haenel, 1974). Corresponding best-fit values of μ and g are assumed to be the correct values. The data in Figure 3, however, were not adequate to obtain a best-fit solution to equation 1 by the indirect method of Lee (1977) without imposing the additional constraint obtained from the sur-

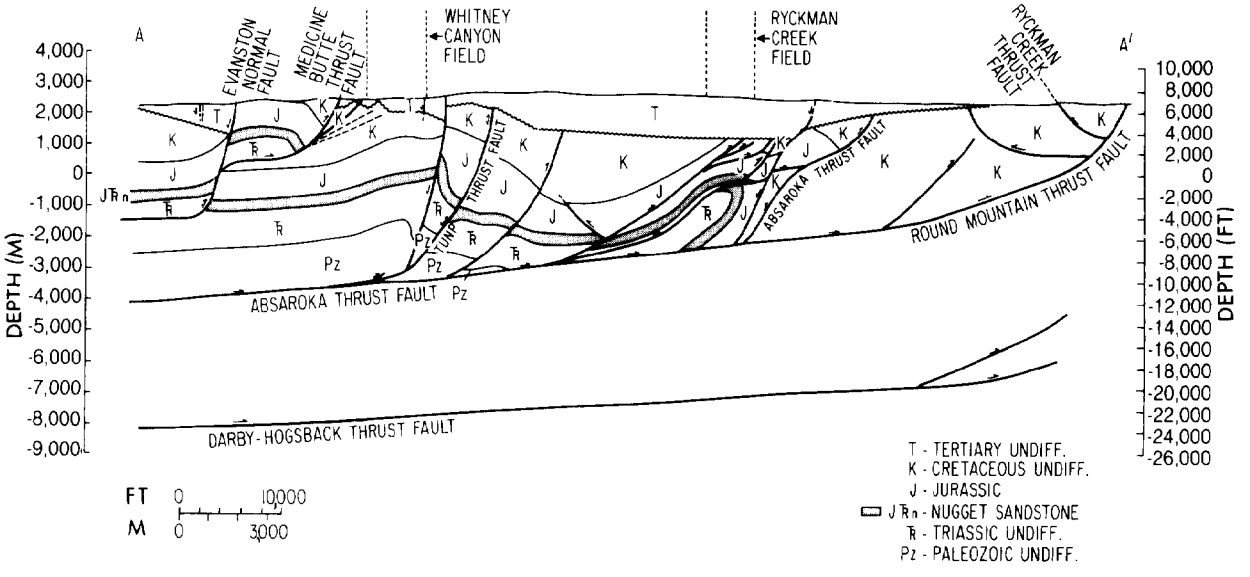

Figure 2—Structural profile across portion of line AA′ (Figure 1) that passes through Whitney Canyon and Ryckman Creek fields.

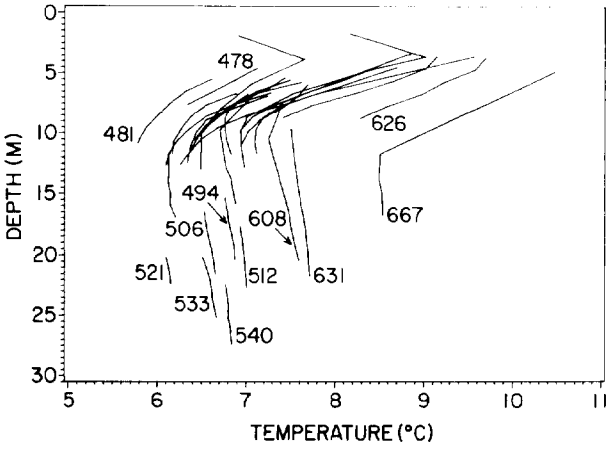

Figure 3—Observed temperature profiles for measured stations. Site location numbers are noted for selected profiles. For additional indication of temperature variation over study area, see Figure 7.

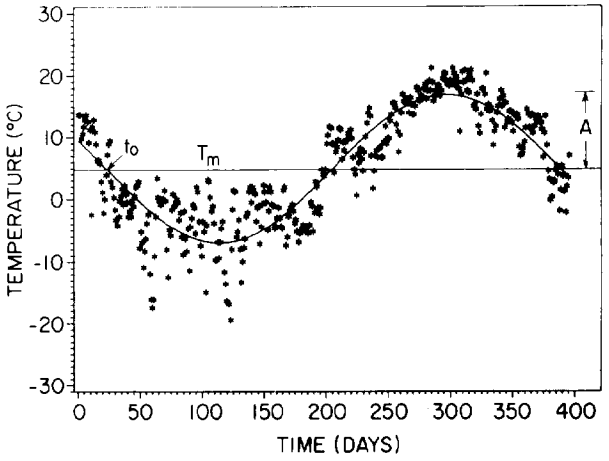

Figure 4—Observed and predicted surface temperature for Evanston, Wyoming, from October 1, 1979 (day 0), to October 31, 1980. Survey was conducted from November 5 (day 401) to November 9 (day 405). T_m = mean annual air temperature, t_o = time when T = T_m, and A = amplitude of the temperature variation.

face air-temperature measurements (Figure 4). The solid curve in Figure 4 is the best-fit sinusoid (period = 1 year) to the data. This allows an estimate of t_o; hence, $t_j - t_o$ could be specified in equation 1 for each station, assuming there is no difference in phase between the annual air-temperature and ground-temperature fluctuations.

The results of successful reduction of the temperature data in Figure 3 are summarized in Table 1. The RMS error for each reduction is quite small, indicating a general agreement of the observed temperatures and theory. Six sites failed to yield minima in RMS error. This can be broadly attributed to a higher degree of geologic variability, such that the simple boundary value theory model just described is insufficient, and/or an inadequate sampling of the temperature distribution with depth at those sites.

In addition to the measurements shown in Figure 3 and

Table 1. Summary of Thermal Results*

Site**	Z_{max}	μ	g	T_s	A	RMSE	μg	k	q
30	1,275	8.4	8.9	6.0	10.8	0.0585	7.5	4.8	4.3
35	1,578	5.3	0.6	6.8	13.0	0.0189	0.3	3.5	0.2
90	1,177	5.0	0.8	6.8	10.1	0.0039	0.4	3.4	0.3
97	995	11.0	21.3	4.6	12.8	0.0020	23.1	5.9	12.6
241	872	12.2	14.5	5.3	13.2	0.0224	17.7	6.4	9.3
280	1,057	5.0	-13.0	7.8	5.8	0.0147	-6.5	3.4	-4.4
310	1,083	4.8	-10.1	6.9	4.2	0.0117	-4.8	3.3	-3.4
370	1,242	6.9	-3.6	6.9	12.2	0.0163	-2.4	4.2	-1.5
425	1,140	12.1	2.2	6.1	6.0	0.0216	2.7	6.4	1.4
481	1,170	5.6	-7.0	7.0	10.2	0.0126	-3.9	3.7	-2.6
486	1,265	7.5	-7.0	7.1	9.4	0.0123	-5.3	4.5	-3.1
503	1,292	10.7	9.2	5.4	7.4	0.0863	9.6	5.8	5.3
506	2,150	13.8	0.2	6.6	14.2	0.0017	0.3	7.1	0.1
512	2,270	14.3	0.2	7.0	7.9	0.0012	0.3	7.3	0.2
524	1,257	13.0	6.2	5.5	12.1	0.0283	8.1	6.8	4.2
603	1,170	7.3	4.4	6.7	11.7	0.0108	3.2	4.4	1.9
608	2,045	6.2	2.5	7.1	7.5	0.0067	1.6	3.9	1.0
631	2,170	7.2	1.3	7.4	8.8	0.0017	0.9	4.3	0.6
667	1,675	8.5	-1.1	8.7	9.7	0.0072	-0.9	4.9	-0.5

*Nomenclature:
μ = thermal diffusivity ($\times 10^{-3}$ cm^2 sec^{-1})
g = thermal gradient ($\times 10^{-4}$ °C cm^{-1})
T_s = mean surface temperature (°C)
A = amplitude of the surface temperature change (°C)
RMSE = root-mean-square error for regression
μg = thermal diffusivity × thermal gradient ($\times 10^{-6}$ °C sec^{-1})
k = thermal conductivity ($\times 10^{-3}$ cal cm^{-1} sec^{-1} $°C^{-1}$)
q = heat flow ($\times 10^{-6}$ cal cm^{-2} sec^{-1})
Z_{max} = maximum depth of measurement (cm)
**Sites 464, 478, 494, 533, 540, and 626, which failed to yield RMSE solutions, are omitted from table. Site 521 contained too few temperature points to attempt solution.

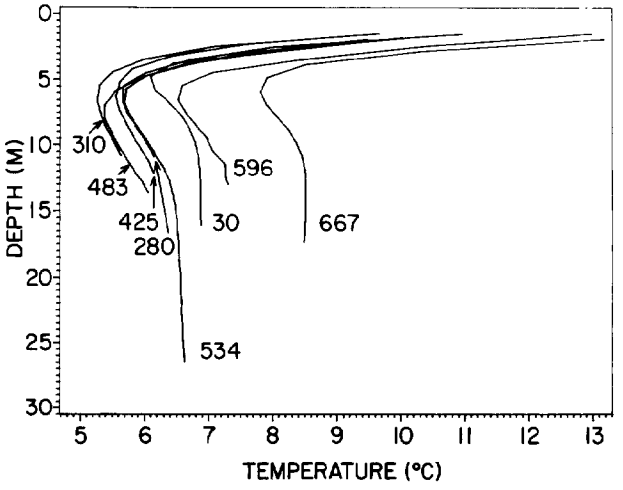

Figure 5—Observed temperature profiles with site location numbers for second survey.

Table 1, the study area was revisited in July 1981, when two new sites were measured and six sites were remeasured. For these measurements (Figure 5), more depth points were sampled and at a more uniform distribution. This resulted in seven of the eight sites yielding successful data reductions solely employing the indirect method of Lee (1977) without imposing additional constraints. These results are summarized in Table 2.

RESULTS

The principal results from Table 1 are plotted with respect to site location along line AA′ in Figure 6 (open symbols). The site location numbers in the data tables correspond to seismic shot-hole numbers, which decrease from 700 to 0 west to east along AA′. This scale is included on all data profiles along AA′ for site location purposes. Figure 6A shows the variation in the product of thermal diffusivity and thermal gradient (μg) across the study area, Figure 6B the thermal gradient (g), and Figure 6C the thermal diffusivity (μ). In Figures 6A and 6B, a cubic spline has been fit to the data. It is evident that the site-to-site variation in μg and g are almost identical; however, the variation in μ (Figure 6C) is comparatively much more random and of much lower magnitude. This implies that the lateral variations in thermal diffusivity, despite a factor of 4 range of variation, are a minor influence in the distribution of steady-state isotherms. Thus, a mechanism capable of considerably larger magnitude heat transport than possible by conduction alone must be at work, assuming there are no large sources of heat such as magma bodies at shallow depth.

The distribution of values shown in Figure 6A and B indicates relative maxima in μg and g situated west of site 500 and centered around site 580, and east of site 280, centered around site 160. In the interval between sites 280 and 500, lower, predominately negative values of g and hence μg were found. These will be discussed shortly. Also plotted in Figure 6 are the corresponding parameters from Table 2 obtained from the measurements made the following summer (solid symbols). Despite the fact that the two sets of measurements were made seasonally out of phase, there is generally good agreement of the second set of measurements with either the original measurements or the original trend (curves). The most noteworthy difference between first- and second-generation values occurs at site 280, where lower and more negative values of μ and g, respectively, are obtained from the repeated measurement. The difference is most likely due to differences in sampling depths for the temperature measurements between the two surveys (see Figure 12, discussed later). At several sites, the shallow depths were inadequately sampled during the first survey. Still, site 280 produced the lowest, most negative gradient of all sites for either set of measurements.

In Figure 7, the temperature profiles for several depths are given. These were computed by inserting values of the parameters T_s, μ, g, and A for each station in Table 1 into equation 1. A spline, mathematically the same as in Figures 6A and 6B, has been fitted through the temperature profiles in order to compare them with the profiles of μg and g. For depths 1, 4, and 10 m, the temperature profiles depart significantly both from each other and from the trends in μg and g. This is due to the interplay of the time-varying component of the vertical temperature profile

Table 2. Summary of Thermal Results for Second Survey*

Site**	μ	g	T_s	A	RMSE	μg	k	q
30	4.1	1.5	6.7	10.1	0.0095	0.6	3.0	0.5
280	9.6	-16.7	8.1	10.4	0.1063	-16.0	5.3	-8.9
310	6.6	-9.2	6.6	9.1	0.1163	-6.1	4.1	-3.8
425	6.4	2.8	5.8	6.6	0.0505	1.8	4.0	1.1
534	8.5	1.5	6.2	9.5	0.0239	1.3	4.9	0.7
596	4.2	6.5	6.5	13.4	0.0601	2.7	3.1	2.0
667	4.5	0.8	8.4	13.6	0.0302	0.4	3.2	0.3

*Nomenclature:
μ = thermal diffusivity ($\times 10^{-3}$ cm^2 sec^{-1})
g = thermal gradient ($\times 10^{-4}$ °C cm^{-1})
T_s = mean surface temperature (°C)
A = amplitude of the surface temperature change (°C)
RMSE = root-mean-square error for regression
μg = thermal diffusivity × thermal gradient ($\times 10^{-6}$ °C sec^{-1})
k = thermal conductivity ($\times 10^{-3}$ cal cm^{-1} sec^{-1} °C^{-1})
q = heat flow ($\times 10^{-6}$ cal cm^{-2} sec^{-1})
**Site 483, which failed to yield RMSE solution, is omitted from table.

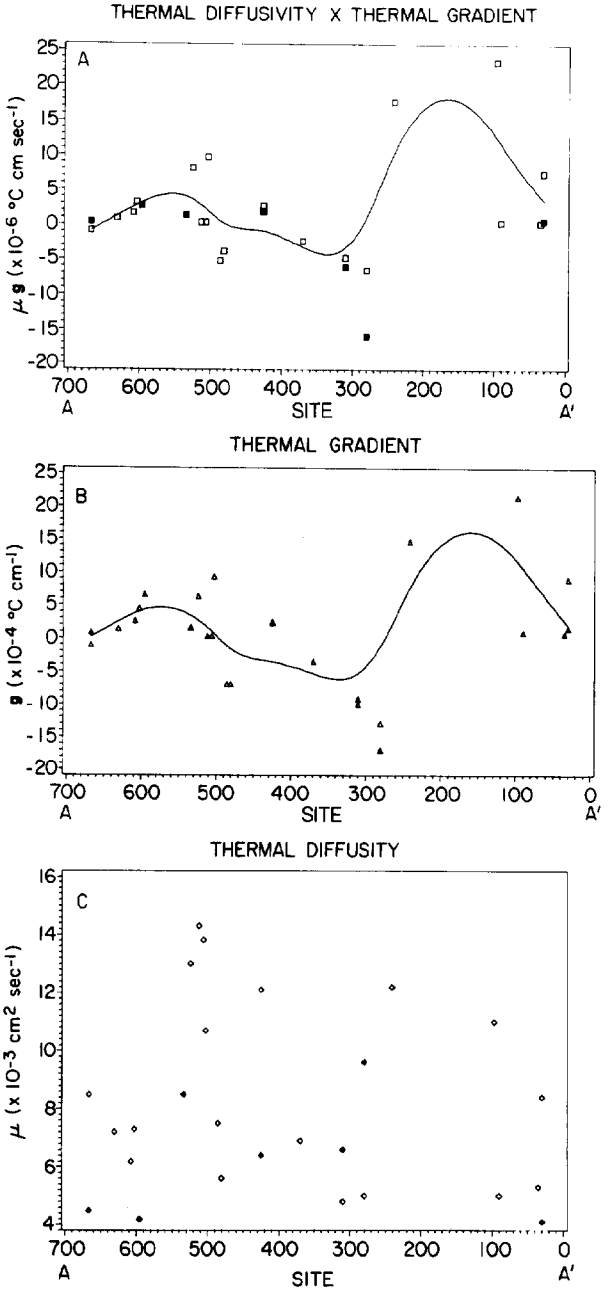

Figure 6—Summary of thermal result vs. site location. Locations are on decreasing scale from 700 to 0 projected on line AA′ (Figure 1). (A) Values of μg (thermal diffusivity × thermal gradient); (B) thermal gradient (g); and (C) thermal diffusivity (μ). Open symbols are measurements from first survey (Table 1); solid symbols are from second survey (Table 2). Spline (curves) in A and B are mathematically identical and computed using only data from first survey.

with the steady-state component. Owing to lateral variations in conditions at the surface (e.g., insolation, thermal properties) from station to station, the temperature profiles in the upper 30 m (98 ft) or so become highly variable and depth-dependent. In this particular area, it is not until depths of the order of 60 m (197 ft) are reached (see Figure 7) that the temperature profiles reflect the variations in μg and g (Figures 6A, B). The temperature profile for 60 m (197 ft) is an extrapolated profile that is deeper than any of the thermal measurements (see Figure 3). Hence, Figures 6A, 6B, and 7 illustrate how computed profiles of μg, and in the present example also g, supposedly reflect the thermal regime below the depth of measurement. The present measurements were made in a thermally complex interval where a survey of temperature at a given depth alone ($z_i <$ 60 m, such as those described in Chapter 4 of Kappelmeyer and Haenel, 1974) would lead to ambiguous results. In their survey of the San Sebastian oil and gas field, Tierra del Fuego, Zielinski and Bruchhausen (1983) showed that the temperature profile at 1.2 m (4 ft) reflected the general trend in μg (i.e., higher values over the field) and, therefore, the temperatures at depth. However, as was discussed earlier, their study area was specifically chosen to minimize lateral variations in surface and near-surface conditions that affect shallow temperatures.

In order to obtain profiles of μg from their data, it was necessary for Zielinski and Bruchhausen (1983) to normalize solutions of equation 1 to constant values of T_s and A. These again were not expected to vary greatly across their particular study area. In addition, they suggested that more random error might be associated with the estimate of A so the normalization to T_s might be more appropriate. This appears to be the case for the present data set. In Figure 8, the values of T_s and A for the sites in Table 1 are plotted as histograms. The range of values of A is significantly greater than that of T_s, such that it was not possible to select a single value of A encompassed by a large enough number of sites for normalization. Normalization to T_s = 6.9 (the median value) was possible, however.

Results for all sites for which solutions to equation 1 could be obtained with T_s = 6.9 are summarized in Table 3. In Figure 9 the values of μg for each site are plotted vs. site number along with the cubic spline for the "best-fit" μg (replotted from Figure 6A). The data points appear to be consistent with the trend of the best-fit data with two notable exceptions—sites 97 and 241 (Table 1; Figure 6A). The normalized data in Table 3 and Figure 9 would indicate only a gradual increase in μg east of site 300. The RMS error for sites 97 and 241, however, is significantly greater than the best-fit error, so that the best-fit values are probably more reliable. Despite this discrepancy, 15 of the 17 points in Figure 9 are consistent with the best-fit trend (curve) even though real variations in T_s on theoretical grounds should be much larger than those for the Zielinski and Bruchhausen (1983) data set. The two most likely causes for increased site-to-site variation in the mean annual surface temperature (T_s) in the Wyoming study area are larger variations in ground cover, which ranged from sparse grasses to groves of deciduous trees, and increased topographic relief (Figure 10). The major effect of the latter is the accompanying variation in slope. All of the above cause variations in exposure to solar radiation, which plays a major role in controlling ground temperature. This exercise in support of the data analysis presented in Zielinski and Bruchhausen (1983) imparts a warning. Normalization to T_s in an area where real variations in T_s are expected and/or exist could lead to suppression (or erroneous amplification) of the relative heat-flow (μg) signal. The effect of normalization on sites 97 and 241 is probably an example of such suppression.

Table 3. Thermal Results for $T_s = 6.9°C$ Normalization*
(First Survey)

Site	μ	g	A	RMSE	μg
30	6.1	1.5	8.2	0.3557	0.91
35	4.7	-0.3	16.7	0.0312	-0.1
90	4.7	-0.2	11.5	0.0052	0.0
97	8.9	0.2	7.8	0.0254	0.2
241	13.8	-3.0	9.4	0.0388	-4.1
280	8.1	-0.4	5.7	0.0233	-3.3
292	14.6	-0.9	4.2	0.0442	-1.3
310	4.8	-10.0	4.2	0.0117	-4.8
370	6.8	-3.0	12.2	0.0164	-2.0
425	9.9	-4.4	4.4	0.0241	-4.4
481	5.9	-5.6	9.6	0.0129	-3.3
486	8.0	-5.6	9.2	0.0131	-4.4
494	11.0	0.0	13.5	0.0046	0.0
503	6.0	-2.0	2.0	0.3734	-1.2
524	11.1	-4.7	8.8	0.0429	-5.4
603	7.1	3.1	11.4	0.0120	2.2
608	8.6	3.6	7.2	0.0771	3.1

*Nomenclature:
T_s = mean surface temperature (°C)
μ = thermal diffusivity ($\times 10^{-3}$ cm^2 sec^{-1})
g = thermal gradient ($\times 10^{-4}$ °C cm^{-1})
A = amplitude of the surface temperature change (°C)
RMSE = root-mean-square error for regression
μg = thermal diffusivity × thermal gradient ($\times 10^{-6}$ °C sec^{-1})

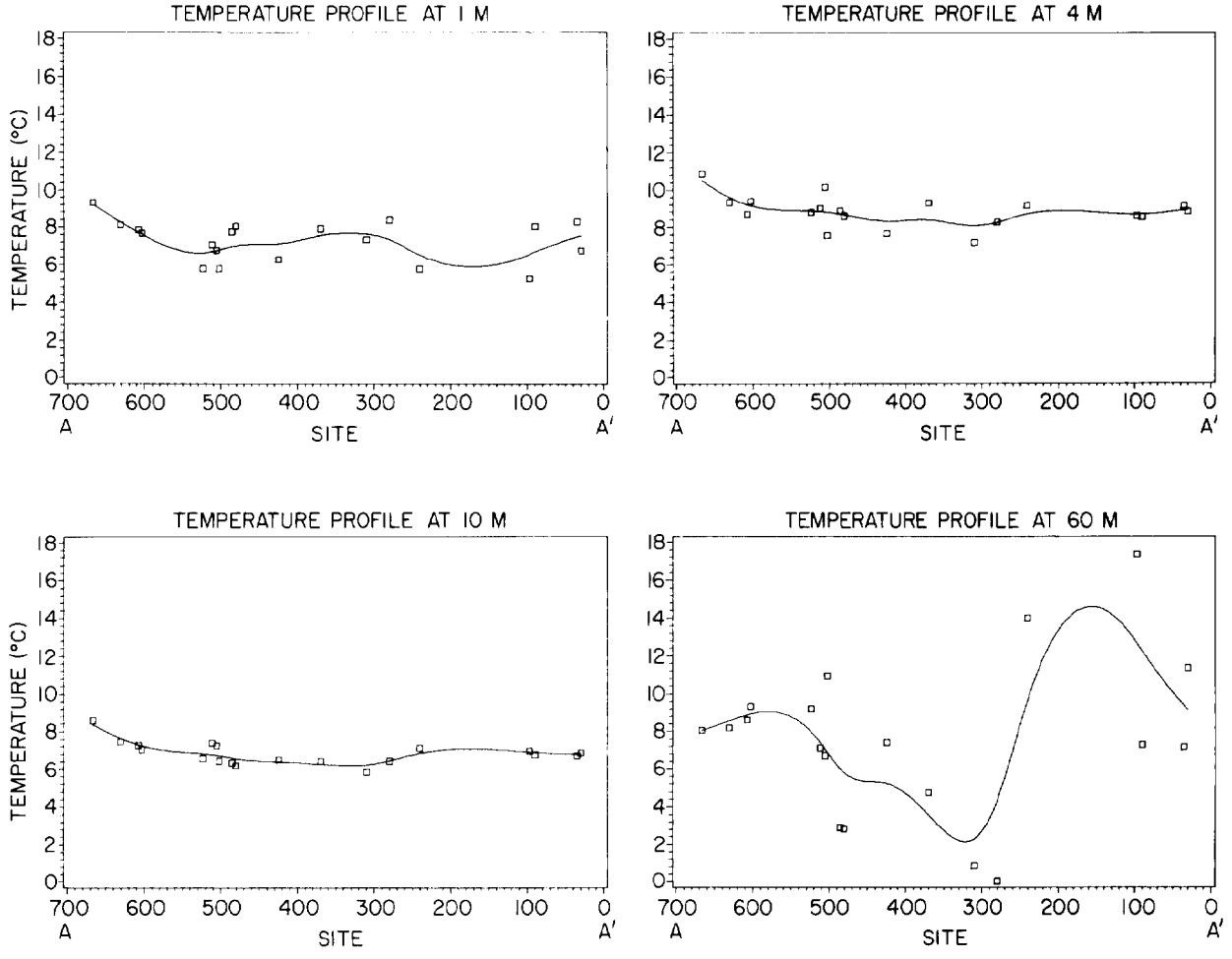

Figure 7—Theoretical temperature profiles (computed from Table 1) for various depths along line AA′ (Figure 1) using mathematically same spline used in Figures 6A and 6B. Site location numbers decrease from 700 to 0 (horizontal scales) along AA′.

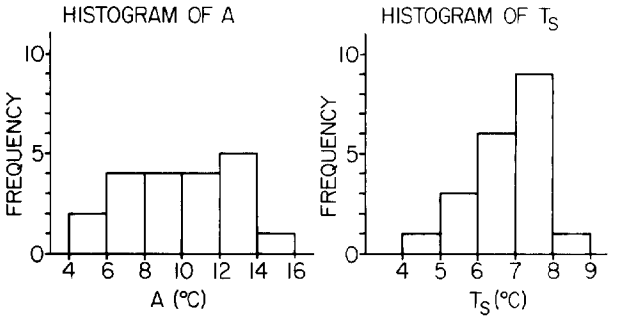

Figure 8—Histograms for T_s (mean annual surface temperature) and A (amplitude of the mean annual surface-temperature variation) from values given in Table 1.

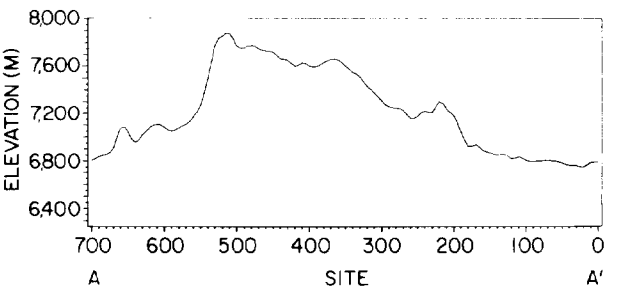

Figure 10—Topography along line AA′ (Figure 1) vs. site location on decreasing scale from 700 to 0.

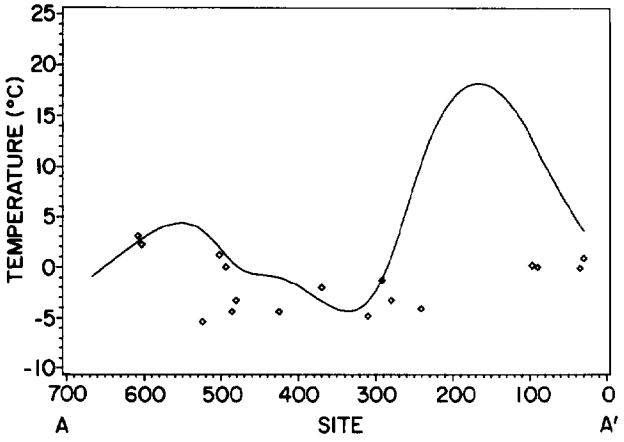

Figure 9—Values of μg normalized to T_s = 6.9°C (Table 3) along line AA′ (Figure 1) vs. site location on decreasing scale from 700 to 0. Smooth curve is spline from Figure 6A (fit through the "best fit" μg of Table 1).

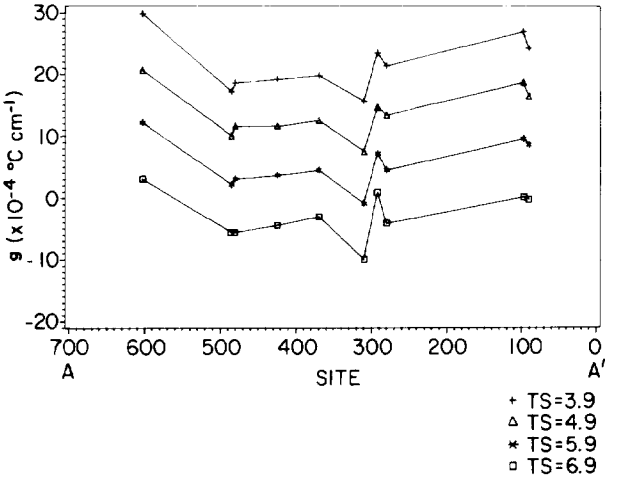

Figure 11—Values of g (thermal gradient) for various normalizations to T_s vs. site location on decreasing scale from 700 to 0. Only sites that had values of g for all normalization to T_s are plotted.

The final topic to be addressed in this section is the observation of negative, supposedly steady-state temperature gradients (Tables 1, 2, 3; Figure 6B). The absolute accuracy of the values of gradient (and diffusivity for that matter) is not well established, and it is not clear that more than the relative differences between sites are significant. For example, Figure 11 shows values of g for sites normalized to different values of T_s in 1°C (1.8°F) increments (only those sites yielding values of g for all normalizations are plotted). For T_s = 6.9 (the median value, Figure 8), most values in Figure 11 are negative, but for T_s = 5.9 and lower, values of g become positive. For the most part, relative differences are preserved. There is, however, a dramatic increase in RMS error for the lower T_s value normalization, which leads us to believe that this effect cannot provide the total explanation and that at least some of the negative gradients are real. Sites 280 and 310, for example, were both measured twice (Tables 1, 2), and in each instance yielded decidedly negative gradients. Furthermore, the measurements were taken seasonally out-of-phase so that the negative gradients existing in the upper 20 m (66 ft) are not a totally transient phenomenon. The temperature data for these stations are shown in Figure 12 along with fitted curves and the average gradients (dashed line) for both first and second sets of measurements. The bar on the temperature axis indicates the range in mean annual ground-surface temperature (T_s) computed from both sets of measurements.

The zone of predominately negative gradients occurs in a zone of highest topographic elevation (Figures 6B, 10). In terms of classic concepts in hydrology, topographically high areas often form zones of regional ground-water recharge (e.g., Hitchon, 1969). The negative gradients might result from a complex thermal interaction of the seasonal temperature wave and the average yearly downward transport of heat by descending ground water. The negative gradient observed by Diment (1967) in the upper portion of a deep borehole was ascribed to the downward conduction of heat from a building situated over the borehole. Similarly, the negative gradients observed in Wyoming may be restricted to shallower depths and may not persist much deeper than the measured depth interval. They may persist, however, year round in "quasisteady state" as suggested by Figure 12. One further observation which can be made regarding the origin of the negative gradients is that, on the average, decidedly positive gradients have a lower T_s than those gradients which are decidedly negative. This can be seen in Figure 13, which contains a plot of the steady-state temperature profile (T_s + gz) for each site (Table 1) from z = 0 to the maximum

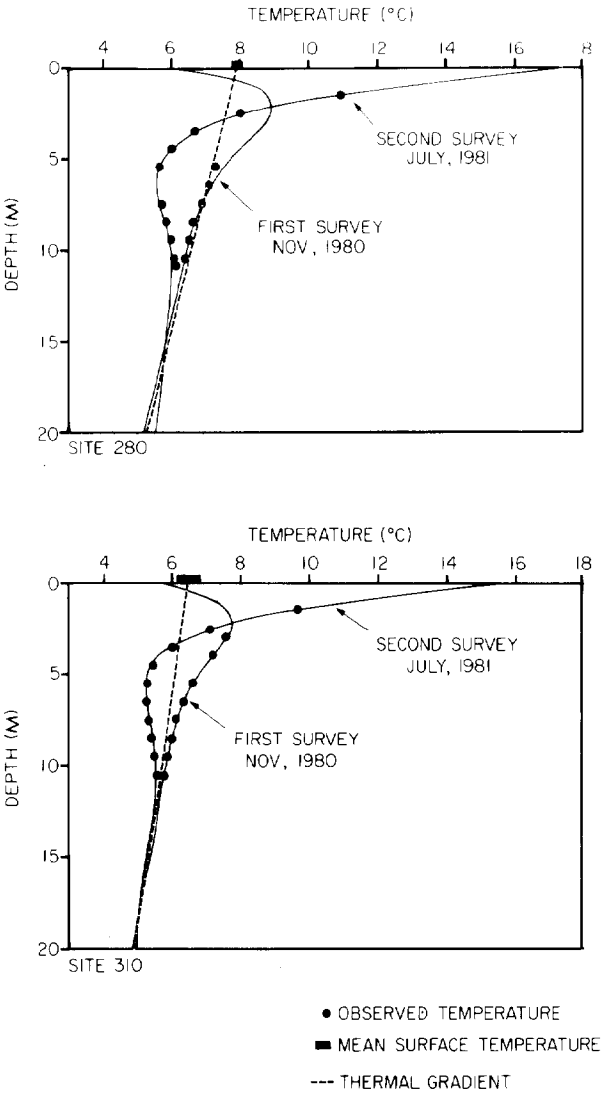

Figure 12—Temperature profiles for sites 280 and 310 from first and second surveys. Solid dots are observed temperature data with fitted curve (solid line), and dashed curve is estimated equilibrium gradient (from Tables 1 and 2). Solid bar on temperature axis is range in T_s estimated by regression (Tables 1 and 2).

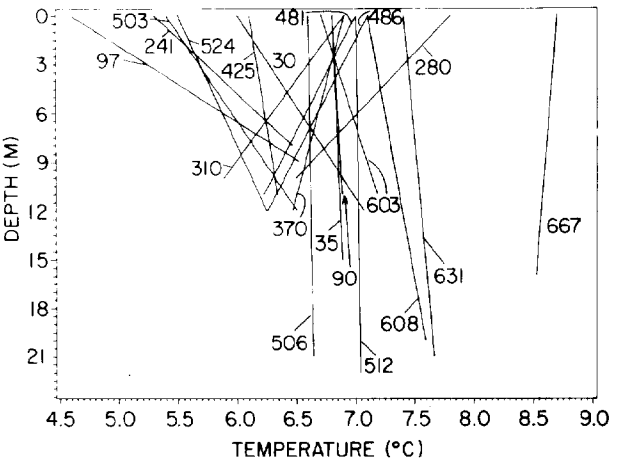

Figure 13—Steady-state temperature profiles ($T_s = gz$) for sites in Table 1. Depth intervals are taken from $z = 0$ ($T = T_s$) to maximum depth measured for each site (Z_{max} in Table 1).

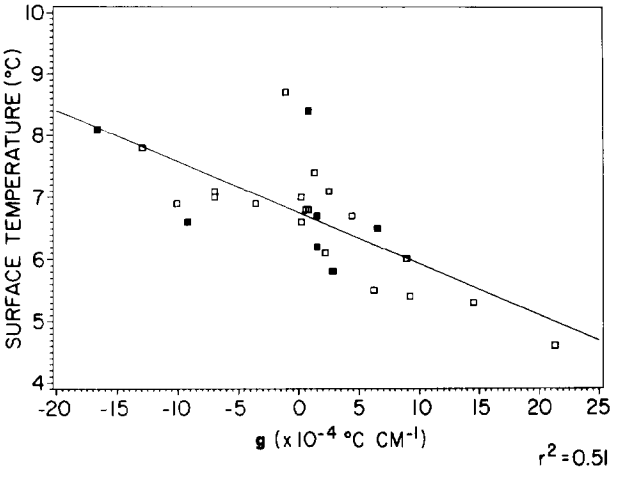

Figure 14—Mean annual surface temperature (T_s) vs. thermal gradient (g). Solid line is least-squares fit to data. Open symbols are measurement from first survey (Table 1); solid symbols are from second survey (Table 2).

depth measured. This trend is obvious in a plot of surface temperature vs. gradient (Figure 14). The average increase in T_s from positive gradient sites to negative gradient sites is 1° or 2°C (1.8° or 3.2°F). This may be evidence of a near-surface temperature excess in the zone of negative gradients. For example, this may imply that if more precipitation falls at higher elevations (where more negative gradients were measured), its temperature averaged over a year may be warmer than the mean ground temperature in at least the upper 30 m (98 ft) or so. Rain falling in the warmer months may be colder than the surface air temperature, yet warmer than the mean annual air temperature of 4.9°C. It may also imply that near-surface ground water moving laterally into the zone of negative gradients may carry a temperature excess prior to descent. All this is quite speculative and not without problems. In any case, if heat transfer by moving ground water plays an important role in establishing and maintaining negative gradients, the trend in T_s vs. g (Figures 13, 14) is more consistent with a major downward component of flow. Rapid upwelling of deeper, warmer waters within the zone of negative gradients might provide a source of excess temperature; however, this process is more likely to create more positive gradients in contrast to negative ones (e.g., Bredehoeft and Papadopulos, 1965).

DISCUSSION

From the data in Tables 1 and 2, it is desirable to obtain at least a crude estimate of the relative heat flow (kg, where k is thermal conductivity) along AA′ (Figures 1, 2). This estimate would allow for a direct comparison of the thermal regime of our study area with that of other areas. Such a comparison is accomplished by converting thermal diffusivity (μ) to thermal conductivity (k) crudely by means of Figure 15, a plot of μ vs. k for a compilation of

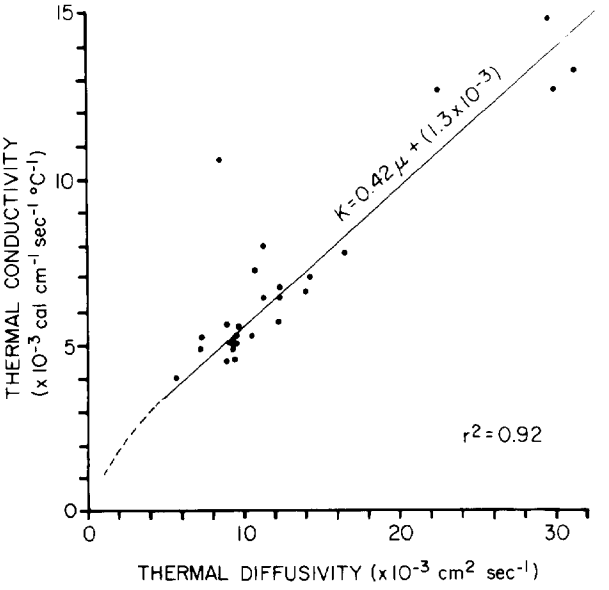

Figure 15—Relationship between thermal diffusivity and thermal conductivity. Dots are data for solid rock taken from Kappelmeyer and Haenel (1974) and straight line is least-squares fit to data. Dashed line is empirical representation of thermal diffusivity vs. thermal conductivity for unconsolidated ocean-bottom sediment derived from Bullard (1963).

measured values (from Kappelmeyer and Haenel, 1974) for a variety of consolidated rocks (solid circles). The dashed curve in Figure 15 is for unconsolidated sediments (Bullard, 1963) and illustrates a possible extrapolation of the data trend toward the origin. Because $\mu \equiv z\ k/\rho c$, where ρ is density and c is heat capacity, a simple straight-line fit to the data implies that, in its effect on μ for most rocks, variations in ρc are small compared with variations in k. The corresponding estimates of k (Figure 15) and, hence, heat flow (q = kg), are given in Tables 1 and 2.

The relative heat-flow values from Table 1 (open symbols) and Table 2 (solid symbols) are plotted as s function of position in Figure 16A. A cubic spline, virtually identical to those in Figures 6A and 6B, has been fitted to the data. For comparison, in Figure 16B, the heat-flow data from the Galapagos spreading center (from Williams et al, 1974) are plotted on the same horizontal and vertical scale with a spline, consistent with their interpretation, fit to those data. Despite the fewer data points and longer wavelength of variation for the Wyoming heat flow, the distribution appears remarkably similar in magnitude and degree of scatter to the Galapagos heat-flow distribution, which has been attributed to hydrothermal convection (Williams et al, 1974). However, buoyancy-driven free convection, which is normally associated with geothermal areas, is not necessarily the mechanism at work in the Wyoming study area. Forced convection due to natural ground-water movement could easily produce the heat-flow distribution in Figure 16A. In view of the magnitude of the heat-flow variation, conductive explanations can be ruled out.

In Figure 17, the general heat-flow trend from Figure 16A is plotted with respect to the simplified subsurface

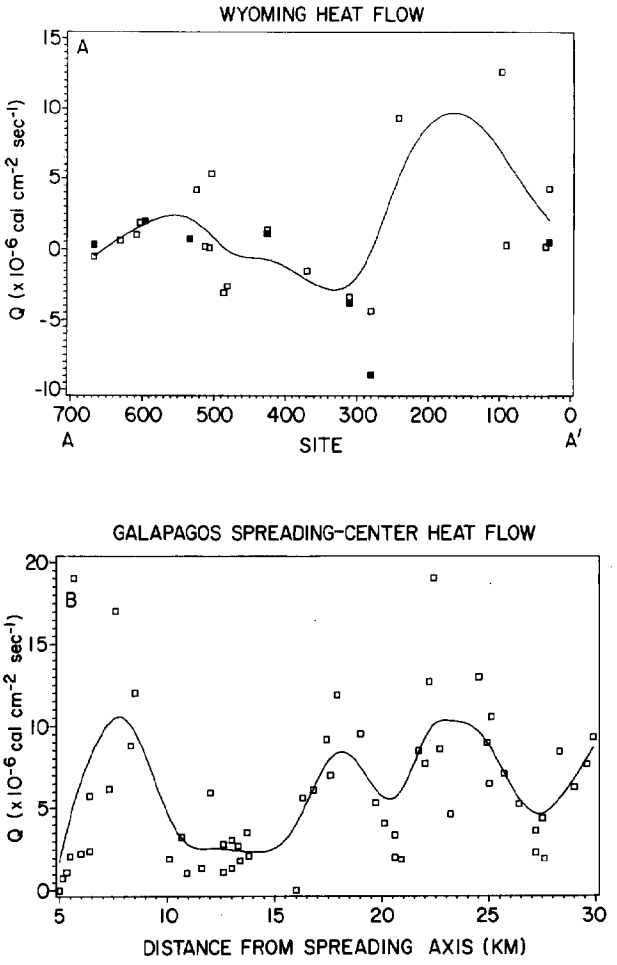

Figure 16—Relative heat flow for Wyoming Overthrust (A) compared to heat flow at Galapagos spreading center (B) (Williams et al, 1974). Curves in A and B are mathematically identical to curves used in Figures 6A, 6B, and 7. Open symbols are measurement from first survey (Table 1); solid symbols are from second survey (Table 2).

structure along line AA′ (Figure 1). Two relative highs are seen in the heat-flow trend. The lower magnitude high to the west appears to be coincident with the Whitney Canyon anticline, which has associated near-vertical faulting. Relatively low heat flow is observed directly over the Ryckman Creek structure; however, the eastern relative heat-flow high occurs directly over the zone where major faults associated with the Ryckman Creek structure project to the surface. If the heat-flow distribution reflects ground-water movement and the relative heat-flow highs delineate zones of surface discharge of warmer, deeper waters, then the principal implication of Figure 17 is that ascending ground water is being focused along major faults that are structurally related.

CONCLUSION AND SPECULATION

From observations resulting from the thermal measurements described in this paper, we illustrated conceptual two-dimensional models for the processes at work in the Wyoming Overthrust belt study area (Figure 18).

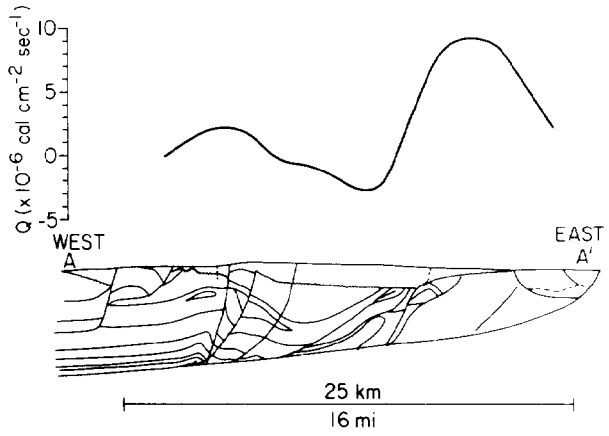

Figure 17—Generalized heat-flow trend from Figure 16A plotted over simplified subsurface structure along line AA′.

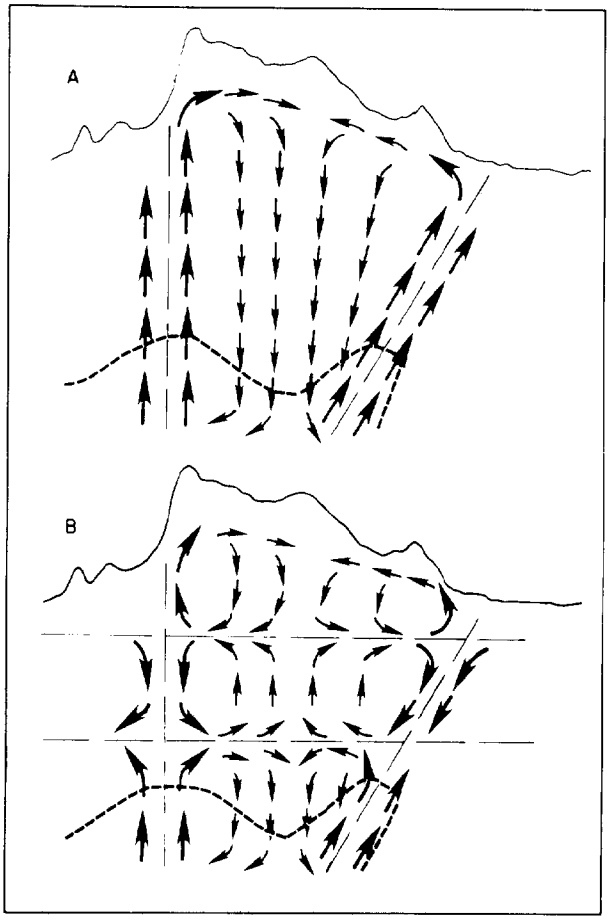

Figure 18—Conceptual two-dimensional model to explain hydrothermics within study area. Surface topography (solid curve) is plotted along with simplified structure (dashed curves) of area's two major fields, Whitney Canyon on left, Ryckman Creek on right. Dashed lines represent fold axes of these structures, along which major subparallel faulting occurs. Large arrows represent high-velocity flow along open channels (major faults along fold axes); smaller arrows signify lower velocity flow in recharge areas (areas of high topography). (A) Direct mixing of ground water originating at structural depths with surface waters. (B) Interaction of deep, intermediate, and shallow ground-water systems.

Although, at present, many details have not been adequately addressed, the models are believed to be reasonably self-consistent and in good agreement with the observations. In Figure 18A, the surface topography along line AA′ (Figure 1) is plotted above a schematic structure surface at depth (dashed curve), which roughly delineates the area's two major fold structures. The fold axis for each structure is drawn as a dashed line with that for Whitney Canyon (left) approximately vertical and for Ryckman Creek (right) oblique as in Figure 2. Both axes intersect the surface where the two major highs in relative heat flow (Figure 16A) are observed.

The arrows in Figure 18A represent hypothetical ground-water flow. The larger arrows aligned parallel with the fold axes represent higher velocity flow channeled along major subparallel faults. In these relatively narrow zones, flow is predominately vertical, giving rise to higher gradients and heat flow where flow reaches the surface. Near the surface, flow becomes lateral into the recharge zone beneath the topographic highlands, where predominately negative temperature gradients (Figure 6B) are observed. With the relative absence of major faulting in this zone, recharge (or downward flow) is illustrated to occur over a larger, more diffuse area and consequently at lower velocity (indicated by smaller arrows). The stagnation of flow at shallow depth in the recharge zone would allow time for any excess heat contained by the ground water, as a result of its rapid ascent in the discharge zones, to be exchanged more efficiently with the ground at shallow depths in the recharge zone. This could help to produce the higher mean annual ground temperatures observed and, coupled with the downward flow component, the negative gradients.

Figure 18A illustrates direct communication of ground water at structural depths with surface waters. Figure 18B, however, suggests the possibility of separate deep, intermediate, and shallow ground-water systems. The important point is that direct communication of waters originating at structural depths with near-surface waters may not be required, provided there is coupling between the systems. If observations of shallow thermal anomalies that reflect deep structure (e.g., Artemenko and Malovitskiy, 1977; Osadchiy et al, 1978; Zielinski and Bruchhausen, 1983) are not fortuitous, then either direct communication of deep and shallow waters (Figure 18A) or coupling between flow systems (Figure 18B) is required.

The models for our study area (Figure 18) illustrate deep ground-water flow into the structures, both of which happen to be hydrocarbon producing. It is interesting to speculate if this sort of flow might have influenced the migration and accumulation of those hydrocarbons (Roberts, 1979; Toth, 1980). Furthermore, Meyer and McGee (1982) recently showed that at least 15 of 22 oil and gas fields from the Rocky Mountain region exhibit thermal anomalies at production depths. For the remaining seven fields, the data (based on drill-stem test temperatures) were inconclusive. Meyer and McGee attributed the most important cause of the anomalies to ascending waters. Our results added to theirs suggest an area encompassing six states where shallow thermal measurements may be used to study and possibly to detect hydrocarbon accumulations prior to deep drilling.

REFERENCES CITED

Artemenko, V. I., and Y. P. Malovitskiy, 1977, Results of a bottom geothermal survey in the Bakhar oil-gas field: Petroleum Geology (USSR), v. 15, 1978, p. 150-152.

Bredehoeft, J. D., and I. S. Papadopulos, 1965, Rates of vertical ground water movement estimated from the earth's thermal profile: Water Resources Research, v. 1, p. 325-328.

Bullard, E. C., 1963, The flow of heat through the floor of the ocean, *in* M. Hill, ed., The sea, v. 3: New York, Wiley-Interscience, p. 218-232.

Diment, W. H., 1967, Thermal regime of a large diameter borehole: instability of the water column and comparison of air- and water-filled conditions: Geophysics, v. 32, p. 720-726.

Hitchon, B., 1969, Fluid flow in the Western Canada sedimentary basin; 1. effect of topography: Water Resources Research, v. 5, p. 186-195.

Kappelmeyer, O., and R. Haenel, 1974, Geothermics with special reference to application: Geoexploration Monographs, series 1, no. 4, Berlin, Gebruder Borntraeger, 238 p.

Lee, T.-C., 1977, On shallow-hole temperature measurements—a test study in the Salton Sea geothermal field: Geophysics, v. 42, p. 572-583.

——— and L. H. Cohen, 1979, Onshore and offshore measurements of temperature gradients in the Salton Sea geothermal area, California: Geophysics, v. 44, p. 206-215.

Meyer, H. J., and H. W. McGee, 1982, Temperature anomalies associated with Rocky Mountain oil and gas fields (abs.): AAPG Bulletin, v. 66, p. 606-607.

Osadchiy, V. G., S. T. Zelizna, R. I. Filyus, and D. V. Sobko, 1978, Geothermal and geochemical anomalies in the Svidnitsko-Kokanov gas-oil field: Petroleum Geology (USSR), v. 15, p. 546-547.

Roberts, W. H., III, 1979, Some uses of temperature data in petroleum exploration: presented to symposium II, Unconventional Methods in Exploration for Petroleum and Natural Gas, Dallas, September 13-14.

Tóth, J., 1980, Cross-formational gravity-flow of ground water: a mechanism of the transport and accumulation of petroleum (the general hydraulic theory of petroleum migration), *in* Problems in petroleum migration: AAPG Studies in Geology 10, p. 121-167.

Williams, D. L., R. P. Von Herzon, J. G. Sclater, and R. N. Anderson, 1974, The Galapagos spreading centre: lithospheric cooling and hydrothermal circulation: Geophysical Journal of the Royal Astronomical Society, v. 38, p. 587-608.

Zielinski, G. W., and P. M. Bruchhausen, 1983, Shallow temperatures and thermal regime in the hydrocarbon province of Tierra del Fuego: AAPG Bulletin, v. 67, p. 166-177.